Control of magnetism across metal to insulator transitions

J. de la Venta,[1,a)] Siming Wang,[1,2] J. G. Ramirez,[1] and Ivan K. Schuller[1]
[1]*Department of Physics and Center for Advanced Nanoscience, University of California, San Diego, La Jolla, California 92093, USA*
[2]*Materials Science and Engineering Program, University of California, San Diego, La Jolla, California 92093, USA*

(Received 3 December 2012; accepted 11 March 2013; published online 28 March 2013)

Magnetic properties (coercivity and magnetization) of ferromagnetic films are strongly affected by the proximity to materials that undergo a metal to insulator transition. Here, we show that stress associated with structural changes across the metal-insulator phase transition in VO_2 and V_2O_3 produces a magnetoelastic anisotropy in ferromagnetic films (Co and Ni) deposited on top of the oxides. The changes in coercivity are as large as 168% and occur in a very narrow temperature range. This effect can be controlled and inverted by the thickness and the deposition temperature of the ferromagnetic films, which is very flexible for important technological applications. © *2013 American Institute of Physics*. [http://dx.doi.org/10.1063/1.4798293]

Controlling the magnetic properties of ferromagnetic (FM) layers without magnetic fields is an on-going challenge in condensed matter with multiple technological implications. External stimuli and proximity effects are the most used methods to control the magnetic properties. Examples of external stimuli are light,[1] and electrical fields.[2–4] Nanostructured materials in proximity with other dissimilar materials are particularly susceptible to external driving forces such as temperature, time varying electric and magnetic fields, electromagnetic waves, pressure, sound, stress, etc. These in turn produce a variety of functionalities, which do not occur in nature. Examples of such structures include: piezoelectric-ferromagnetic,[5–7] ferromagnetic-multiferroic,[8] and ferroelectric-ferromagnetic[9,10] heterostructures. An interesting possibility along these lines is offered by ferromagnets in proximity to materials that undergo a metal-insulator (MIT) and structural phase transition (SPT).[11,12] The SPT and MIT are usually driven by temperature but they may also be driven by current, light and pressure.[13] Thus, if the magnetism of the FM is affected by the proximity to materials that undergo MIT, then tuning the magnetic properties by multiple stimuli may become possible.

Canonical examples of materials that undergo MIT and SPT are the vanadium oxides VO_2 and V_2O_3.[14] VO_2 exhibits a first order phase transition at ~340 K, from a low temperature insulating to a high temperature metallic phase.[13] The resistance changes can be as large as 4 orders of magnitude across the MIT. Concurrent with the MIT there is a structural change from a low temperature monoclinic to high temperature rutile phase.[13] On the other hand, the transition in V_2O_3 at ~160 K is from a low temperature antiferromagnetic insulating phase to a high temperature paramagnetic metallic phase, with a resistance change up to 5 orders of magnitude. The associate SPT is from monoclinic in the insulating phase to rhombohedral symmetry in the metallic phase.[15,16]

In this letter, we show that the magnetic properties of FM films can be tailored and controlled using the SPT and MIT in VO_2 and V_2O_3. We find reproducible changes in the coercivity and magnetization in a variety of configurations. We also show that the magnetic properties can be modified by the deposition conditions and thickness of the ferromagnetic films. This opens up an avenue for the study of ferromagnetic heterostructures and for the development of devices.

The samples were prepared in a high-vacuum sputtering deposition system with a base pressure of 1×10^{-7} Torr. The VO_2 and V_2O_3 films were deposited at 600 °C and at 750 °C, respectively, by RF sputtering of a V_2O_3 target on *r*-cut $(10\bar{1}2)$ sapphire ($\alpha-Al_2O_3$) substrates. The RF magnetron power was kept at 100 W and the total pressure was 4 mTorr. For VO_2 a mixture of ultra-high purity (UHP) Ar and O_2 was used. The oxygen partial pressure was 0.4 mTorr. For V_2O_3 only UHP Ar (4 mTorr) was used as sputtering gas. After recovering the base pressure the Ni was deposited by RF sputtering from a Ni target at two different temperatures: 420 K and 300 K (room temperature, RT). Co was deposited at RT by e-beam evaporation in a vacuum system with a base pressure of 5×10^{-7} Torr. A capping layer of Cu or Al was deposited to prevent oxidization. X-ray diffraction (XRD) was performed with a Bruker D8 Discovery rotating anode diffractometer using Cu Kα radiation. Magnetic characterization was performed using a Quantum Design superconducting quantum interference device magnetometer (SQUID) and a Vibrating Sample Magnetometer (VSM). The R vs. T characteristics were obtained from standard two probe measurements using a constant current source and a nanovoltmeter. Temperature was swept at constant rate of 1 K/min using a Lakeshore 332 temperature controller.

Fig. 1 shows the XRD pattern for bilayers with 100 nm of VO_2 (or V_2O_3) and 10 nm of Ni. The VO_2 Bragg peak could be indexed as the (200) and $(\bar{2}11)$ planes of the monoclinic phase. V_2O_3 grows epitaxially with the substrate along the (012) direction. The instrumental limitations prevent us to discriminate the 10 nm Ni film. However, for Ni films with 50 and 100 nm thicknesses, we were able to determine that the Ni grown at RT is polycrystalline. On the other hand, the Ni film is textured along the (220) direction when deposited at 420 K on top of VO_2. This was concluded after

a)jdelaventa@physics.ucsd.edu

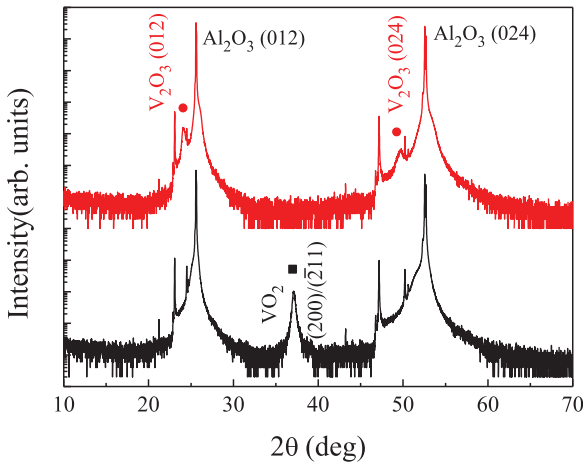

FIG. 1. XRD pattern (Cu Kα, $\theta/2\theta$ geometry) for: (bottom) 100 nm VO_2/10 nm Ni and (top) 100 nm V_2O_3/10 nm Ni. V_2O_3 (dots) and VO_2 (square) diffraction maxima are indexed in the figure. The non-indexed sharp XRD peaks are from the substrate. For visualization the curves are shifted along the Y axis.

extensive XRD studies using $\theta/2\theta$ scans, grazing incidence diffraction, and rocking curves with different sample alignment. Fig. 2(a) shows the XRD pattern focused around the VO_2 Bragg peak at 360 K and at RT for a 100 nm VO_2/10 nm Ni bilayer. Above the SPT, the Bragg peak at 37.27° corresponds to the (011) planes of the rutile phase. Below the SPT, the VO_2 Bragg peak shifted to 37.12° and corresponds to the (200) and ($\bar{2}$11) planes of the monoclinic phase. The evolution of the Bragg peak with the temperature is depicted in Fig. 2(b). Across the MIT transition, the resistance change shows the typical VO_2 thermal hysteresis, Fig. 2(c).

Fig. 3(a) shows the magnetization vs. field curves at different temperatures for a 100 nm VO_2/10 nm Ni bilayer. The most striking effect is the large increase in coercivity (H_C) in a narrow temperature range from 350 to 320 K, black squares in Fig. 3(b). For a comparable 10 nm Ni film there is a not surprising linear dependence of the coercivity with temperature, blue diamonds in Fig. 3(b). For our VO_2/Ni bilayers, the increase in the coercive field from 350 to 320 K is up to 168% (from 88 to 236 Oe). The magnitude of the change in coercivity increases with decreasing Ni thickness, Fig. 3(b), indicating that this is an interface effect. Thus, the change in coercivity can be controlled with the Ni thickness. For instance the 350 to 320 K coercivity increase is 51% and 15% for 50 and 100 nm Ni, respectively. The SPT and MIT in VO_2 at ~340 K, are correlated with the changes in coercivity and magnetization as shown in Fig. 2. The coercivity (Fig. 2(d)) tracks closely the SPT and MIT, (Figs. 2(b) and 2(c)) and shows the same thermal hysteresis.

The changes in magnetic properties across the MIT can also be tuned by the growth conditions. The previous results were obtained when the Ni was grown at 420 K, i.e., on the VO_2 in the metallic rutile phase. When the Ni was deposited at RT on VO_2 in the insulating monoclinic phase, the coercivity change reverses, i.e., decreases by 44% with decreasing the temperature from 350 to 320 K, open symbols in Fig. 4(a). The behavior is opposite for the bilayers with the Ni deposited at 420 K, solid squares in Fig. 4(a). In addition, the magnetization changes with temperature in the two

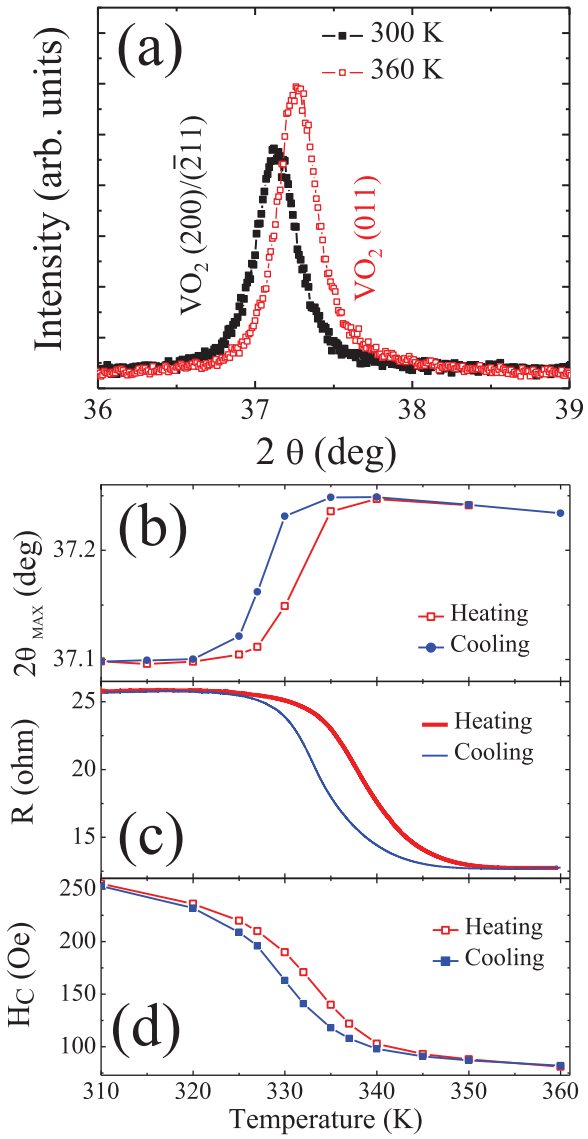

FIG. 2. (a) XRD pattern at 300 and 360 K for 100 nm VO_2/10 nm Ni bilayer. (b) VO_2 Bragg peak position vs. T. (c) R vs. T. (d) Coercivity vs. T.

samples are also opposite as shown in Fig. 4(b). When cooling across the MIT, the magnetization of Ni grown at RT increases, while it decreases for the Ni deposited at 420 K. These changes in the magnetization with temperature may indicate that the Ni is not fully saturated at 1000 Oe, as observed in the inset Fig. 3(b). Another mechanisms as changes in the magnetization saturation due to interatomic rearrangement cannot be discarded. Theoretical calculations have predicted enhanced magnetic moments in metallic surfaces due to variations in the lattice constant.[17,18] Thus, the growth temperature provides an additional reproducible and repeatable control parameter. We measured R vs. T curves as well as XRD at temperatures below and above the transition. The VO_2 MIT and SPT occur in the same way independently of the Ni deposition temperature. Thus, the differences in the magnetic properties of Ni are due to the different Ni structure and how it responds to the stress across the VO_2 MIT.

To investigate the generality of these effects, we studied V_2O_3/FM bilayers using V_2O_3 that shows SPT and MIT at ~160 K.[15,16] Films of 10 nm Ni or Co in proximity to

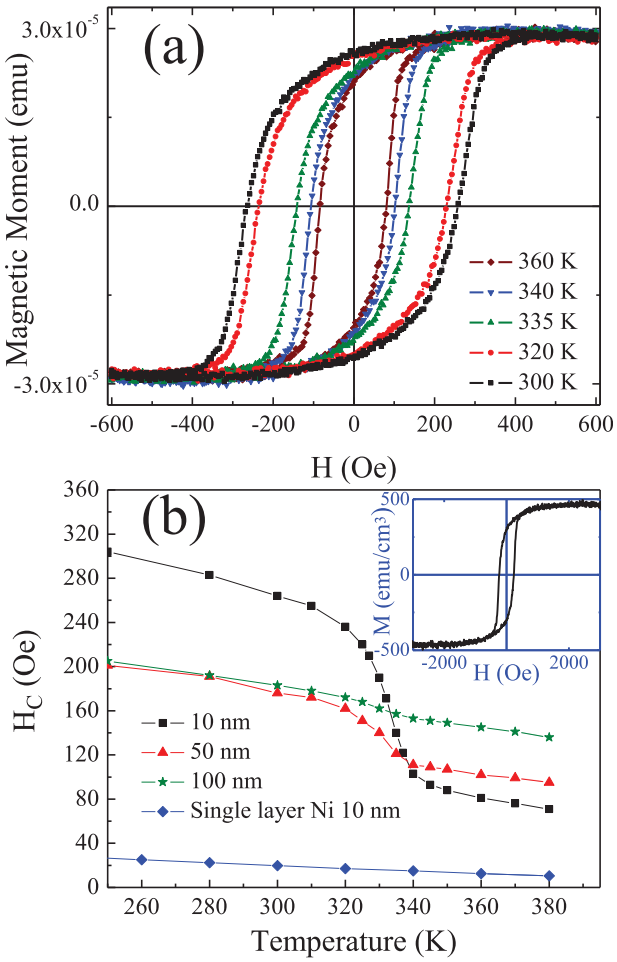

FIG. 3. (a) In-plane hysteresis loops at various temperatures for a 100 nm VO_2/10 nm Ni bilayer. (b) Coercivity vs. temperature for a 10 nm Ni film (blue diamonds) and bilayers of 100 nm VO_2 with different Ni thicknesses: 10 nm (black squares), 50 nm (red triangles), and 100 nm (green stars). The Ni layer was deposited at 420 K. Inset (b) M vs. H at 300 K for the same 100 nm VO_2/10 nm Ni bilayer after diamagnetic background correction and normalization.

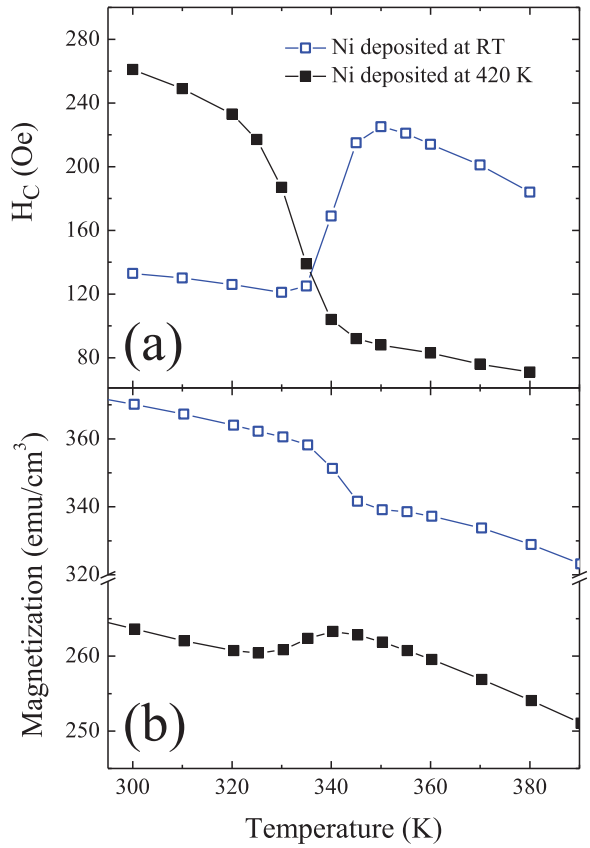

FIG. 4. (a) Dependence of coercivity with temperature for bilayers of 100 nm VO_2 and 10 nm Ni. (b) In plane SQUID magnetization versus temperature measured at 1000 Oe, no diamagnetic correction. Ni layers were deposited at 420 K (solid squares) and RT (empty squares).

100 nm of V_2O_3 behave identically to VO_2 bilayers but at the V_2O_3 MIT temperature, Fig. 5. There is an increase in the coercivity and a decrease in the magnetization between 200 and 140 K. For Ni the coercivity increases by 115%, from 127 to 273 Oe at 200 and 140 K, respectively. The effect is smaller in the case of Co, but an observable coercivity increase from 76 to 89 Oe, inset Fig. 5(a).

These large reproducible effects probably originate from the structural changes across the MIT. The (~0.32%) volume expansion in VO_2 (Ref. 19) or the (1.4%) volume decrease in V_2O_3 (Ref. 20) across the MIT produces epitaxial stress in the FM overlayer. In turn, the stress in the FM layers changes the magnetic properties by the inverse magnetostrictive effect.[21] This interfacial magnetoelastic effect provides a natural explanation for the thickness dependence of the coercivity increase shown in Fig. 3(b). Therefore, a thin Ni film is more sensitive to the interfacial stress and the changes in coercivity are larger than for a thicker film. The observed magnetic behavior is independent of the direction of the in-plane magnetic field, thus ruling out the existence of in-plane axial magnetic anisotropy. These changes in magnetization across the MIT are observed either with an applied field or in remanence. At remanence the temperature was cycled twice and the curves overlap. This overlap in the magnetization curves with thermal cycling indicates the reversibility of the process and confirms that the stress in the FM layer is within the elastic limit.

The lattice distortions in VO_2 and V_2O_3 occur mainly in the V atoms along the c-axis of the rutile and hexagonal basis, respectively. In the low temperature VO_2 phase, the V atoms are displaced along the rutile c-axis to form pairs of V atoms with closer spacing than at high temperature.[19] In V_2O_3, the V-V distance along the c-axis in hexagonal basis is larger in the monoclinic phase compared to the rhombohedral one.[16] These translate into an anisotropic atomic rearrangement on the film plane (011) and (012) for VO_2 and V_2O_3, respectively; the atomic distance increases in one axis and decreases in the other producing an overall shear strain. This strain produces an anisotropic stress in the film deposited on top. In addition to the atomic rearrangement due to the SPT there are two additional parameters, which may affect the interfacial stress in VO_2 samples: the coexistence of the rutile and monoclinic phases across the transition[22] and the presence of twin boundaries in the RT monoclinic phase.[23,24] These effects make it difficult to predict the exact epitaxial stress on the FM produced by VO_2. However, using the FM inverse magnetostrictive properties it is possible to estimate the type and magnitude of stress. Ni and Co have a negative magnetostriction coefficient,[21] so they contract when magnetized. Conversely, the magnetization increases

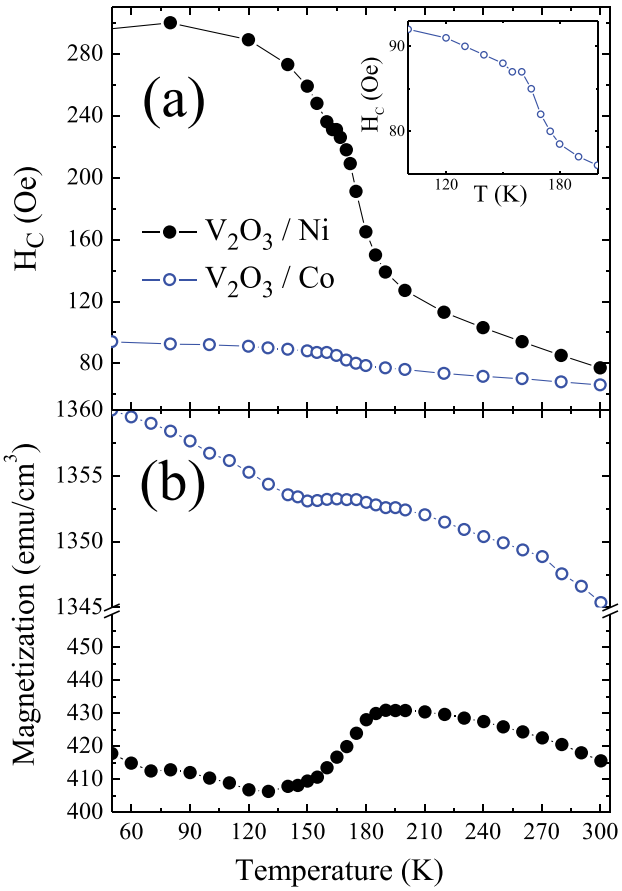

FIG. 5. (a) Dependence of coercivity with temperature for bilayers of 100 nm V_2O_3 and 10 nm Ni (solid dots) and Co (empty dots). (b) In plane SQUID magnetization versus temperature measured at 500 Oe.

(decreases) with compressive (tensile) stress. For Ni deposited at 420 K, the magnetization decreases when cooling across the SPT, Fig. 4(b). In contrast for Ni deposited at RT the magnetization increases in the 350 to 320 K range, Fig. 4(b). Thus, if the ferromagnet is deposited at temperatures above the phase transition, the stress upon crossing the transition has opposite sign than when the ferromagnet is deposited at temperatures below the phase transition.

The magnitude of stress needed to produce the variations in coercivity observed for the 100 nm VO_2/10 nm Ni bilayer (Fig. 3(b)) can be estimated as follows. The coercivity of a FM layer without stress has a linear dependence with temperature. Thus, without any stress the values of the coercivity at 320 K should be 105 Oe. This value is obtained by extrapolating to 320 K, the coercivity values above the SPT, Fig. 3(b). However, the observed value of the coercivity at 320 K is 236 Oe, 128 Oe larger. Assuming that the stress in the film is uniform and that the change in coercivity is caused by the stress anisotropy field given by[21]

$$H_{K\sigma} = \frac{3\lambda_{si}\sigma}{M_S}, \tag{1}$$

where σ is the stress in MPa, λ_{si} is the saturation magnetostriction (for polycrystalline Ni $\lambda_p = -34 \times 10^{-6}$),[21,25] and M_S is the saturation magnetization in G or emu/cm^3, $M_S = 470$ emu/cm^3, inset Fig. 3(b). Thus, to produce an anisotropy field of 128 Oe by this effect it is necessary to have $\sigma = 589$ MPa. This value is close to those obtained from stress measurements in single VO_2 films across the SPT,[26] supporting the idea that the effect is due to stress transferred from VO_2 to Ni. A similar calculation can be made for a V_2O_3 / Ni bilayer. At 120 K the difference between the real value of coercivity and the one extrapolated from the linear behavior is 120 Oe. Therefore, using the same value of M_S for Ni the stress value obtained is $\sigma = 553$ MPa, similar to the one found VO_2. The differences between the Ni and Co bilayers observed in Fig. 5 arise from the different magnetic properties. M_S for Co is approximately three times larger than Ni. The λ_{si} coefficient for polycrystalline Co is also negative but three times smaller than Ni.[21] Thus, according to Eq. (1), the stress induced anisotropy in Ni is up to nine times larger than Co for the same applied stress.

In summary, we have shown that proximity effects provide a control mechanism of the magnetic properties of ferromagnetic layers grown on materials that undergo a MIT. Interfacial stress across the SPT is responsible for the magnetoelastic coupling, which causes large changes in the coercivity and noticeable modifications of the magnetization due to an inverse magnetostrictive effect. The thickness and the deposition conditions of the FM Ni on the VO_2 provide the means by which it is possible to control coercivity and magnetization. The large change in the coercivity in a very narrow temperature range above the room temperature opens possibilities for technological applications. The extension of the study to V_2O_3 and Co shows that the effect is general for other FMs in contact with materials that undergo SPT.

The magnetism aspects of this work were supported by the Office of Basic Energy Science, U.S. Department of Energy, under Grant No. DE FG03-87ER-45332 and the oxide related science by the AFOSR Grant No. FA9550-12-1-0381.

[1] A. Kirilyuk, A. V. Kimel, and T. Rasing, Rev. Mod. Phys. **82**, 2731 (2010).
[2] H. Ohno, D. Chiba, F. Matsukura, T. Omiya, E. Abe, T. Dietl, Y. Ohno, and K. Ohtani, Nature (London) **408**, 944 (2000).
[3] A. Chernyshov, M. Overby, X. Liu, J. K. Furdyna, Y. Lyanda-Geller, and L. P. Rokhinson, Nat. Phys. **5**, 656 (2009).
[4] L. P. Rokhinson, M. Overby, A. Chernyshov, Y. Lyanda-Geller, X. Liu, and J. K. Furdyna, J. Magn. Magn. Mater. **324**, 3379 (2012).
[5] S. Sahoo, S. Polisetty, C.-G. Duan, S. S. Jaswal, E. Y. Tsymbal, and C. Binek, Phys. Rev. B **76**, 092108 (2007).
[6] A. Brandlmaier, S. Geprägs, M. Weiler, A. Boger, M. Opel, H. Huebl, C. Bihler, M. S. Brandt, B. Botters, D. Grundler, R. Gross, and S. T. B. Goennenwein, Phys. Rev. B **77**, 104445 (2008).
[7] S. Geprägs, A. Brandlmaier, M. Opel, R. Gross, and S. T. B. Goennenwein, Appl. Phys. Lett. **96**, 142509 (2010).
[8] J. T. Heron, M. Trassin, K. Ashraf, M. Gajek, Q. He, S. Y. Yang, D. E. Nikonov, Y.-H. Chu, S. Salahuddin, and R. Ramesh, Phys. Rev. Lett. **107**, 217202 (2011).
[9] M. K. Lee, T. K. Nath, C. B. Eom, M. C. Smoak, and F. Tsui, Appl. Phys. Lett. **77**, 3547 (2000).
[10] A. Mardana, S. Ducharme, and S. Adenwalla, Nano Lett. **11**, 3862 (2011).
[11] N. F. Mott, *Metal-Insulator Transitions* (Taylor & Francis, London, 1990).
[12] D. Adler, Rev. Mod. Phys. **40**, 714 (1968).
[13] M. Imada, A. Fujimori, and Y. Tokura, Rev. Mod. Phys. **70**, 1039 (1998).
[14] F. J. Morin, Phys. Rev. Lett. **3**, 34 (1959).
[15] R. M. Moon, J. Appl. Phys. **41**, 883 (1970).
[16] P. D. Dernier and M. Marizio, Phys. Rev. B **2**, 3771 (1970).
[17] A. J. Freeman and R.-Q. Wu, J. Magn. Magn. Mater. **100**, 497 (1991).
[18] T. M. Hattox, J. B. Conklin, J. C. Slater, and S. B. Trickey, J. Phys. Chem. Solids **34**, 1627 (1973).
[19] C. H. Griffith and H. K. Eastwood, J. Appl.Phys. **45**, 2201 (1974).

[20]A. I. Frenkel, E. A. Stern, and F. A. Chudnovsky, Solid. State. Commun. **102**, 637 (1997).
[21]B. D. Cullity and C. D. Graham, *Introduction to Magnetic Materials* (John Wiley & Sons, Hoboken, New Jersey, 2009) p. 250, 251, 256, and 318.
[22]M. M. Qazilbash, A. Tripathi, A. A. Schafgans, B. J. Kim, H. T. Kim, Z. Cai, M. V. Holt, J. M. Maser, F. Keilmann, O. G. Shpyrko, and D. N. Basov, Phys. Rev. B **83**, 165108 (2011).
[23]T. Yang, R. Aggarwal, A. Gupta, H. Zhou, R. J. Narayan, and J. Narayan, J. Appl. Phys. **107**, 053514 (2010).
[24]Y. Zhao, J. H. Lee, Y. Zhu, M. Nazari, C. Chen, H. Wang, A. Bernussi, M. Holtz, and Z. Fan, J. Appl. Phys. **111**, 053533 (2012).
[25]We used the values of λ_{si} for polycrystalline Ni $\lambda_p = -34 \times 10^{-6}$ for our calculations. For single crystals the values are very similar, $\lambda_{100} = -46 \times 10^{-6}$, $\lambda_{110} = -33 \times 10^{-6}$, and $\lambda_{111} = -24 \times 10^{-6}$ as a function of the crystal direction. B. D. Cullity and C. D. Graham, *Introduction to Magnetic Materials* (John Wiley & Sons, Hoboken, New Jersey, 2009), p. 250.
[26]B. Viswanath, C. Ko, and S. Ramanathan, Scr. Mater. **64**, 490 (2011).